analytical chemistry

pubs.acs.org/ac Article

Capsulation of AuNCs with AIE Effect into Metal−Organic Framework for the Marriage of a Fluorescence and Colorimetric Biosensor to Detect Organophosphorus Pesticides

Yue Cai,[‖] Hongshuai Zhu,[‖] Weichi Zhou, Ziyin Qiu, Congcong Chen, Aori Qileng,* Kangshun Li,* and Yingju Liu*

Cite This: *Anal. Chem.* 2021, 93, 7275−7282 Read Online

ACCESS | Metrics & More | Article Recommendations | Supporting Information

ABSTRACT: Organophosphorus pesticides (OPs) can inhibit the activity of acetylcholinesterase (AChE) to induce neurological diseases. It is significant to exploit a rapid and sensitive strategy to monitor OPs. Here, a metal−organic framework (MOF) acted as a carrier to encapsulate AuNCs, which can limit the molecular motion of AuNCs, trigger the aggregation-induced emission (AIE) effect, and exhibit a strong fluorescence with a fluorescence lifetime and quantum yield of 6.83 μs and 4.63%, respectively. Then, the marriage of fluorescence and colorimetric signals was realized on the basis of the dual function of the enzymolysis product from AChE and choline oxidase (CHO) on AuNCs@ZIF-8. First, it can decompose ZIF-8 to weaken the restraint on AuNCs, and thus the fluorescence receded. Second, it can be used as a substrate for the peroxidase mimics of the released AuNCs to oxidize 3,3′,5,5′-tetramethylbenzidine (TMB) and a visible blue appeared. Thus, on the basis of the inhibition of AChE activity by OPs, a fluorescence−colorimetric dual-signal biosensor was established. In addition, colorimetric paper strips were exploited to realize a visual semiquantitative detection, and a smartphone APP was developed to make the visualization results more precise and realize real-time supervision of pesticide contamination.

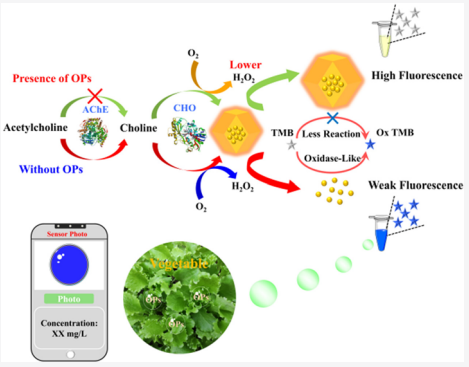

1. INTRODUCTION

Organophosphorus pesticide (OPs), the mainstay of the development of the pesticide industry, are widely used in agricultural production for the reason that it has the advantages of dealing with pests effectively to increase crop yields.[1−3] Unfortunately, the misuse of OPs has caused pollution of water resources, fruits, vegetables, and processed foods, which brings great damage to the ecological environment and human health. The serine on AChE can bind with OPs to cause phosphorylation, hence inhibiting the activity of AChE and preventing the breakdown of neurotransmitters. A series of health problems such as paralysis, respiratory failure, and even death may be found.[4−7] The China Food Safety Organization has established the marginal value of various OPs in different foods. For instance, the maximum residues of acephate in fruits and vegetables are from 0.2 to 1 mg/kg. The maximum dose of phosmet is about 0.05 mg/kg in potato, 0.5 mg/kg in paddy rice, and 0.2 mg/kg in nuts (GB 2763-2019). As a consequence, it is crucial to establish a rapid and convenient method to monitor OPs.

Hitherto, many analytical methods including enzyme-linked immunosorbent assays,[8,9] gas chromatography−mass spectrometry,[10] high-performance liquid chromatography,[11] and electrochemical methods[12,13] have been established to detect OPs. However, it is regrettable that these methods are somewhat insufficient. The immunoassay method has certain limitations due to the high antibody production cost and susceptibility to temperature and pH. Laboratory-based chromatography has the merits of high sensitivity and good selectivity, but it is time-consuming, expensive, and not suitable in field detection. For the past few years, there has been a tendency to monitor OPs through fluorescence analysis due to its high sensitivity, low cost, and easy imaging.[14−16]

Among the fluorescent probes, gold nanoclusters (AuNCs) have attracted great attention in biosensing and biomedicine due to its facile synthesis and good biocompatibility.[17−19] However, the luminous performance of AuNCs is far inferior to those of the developed fluorophores (quantum dots, for instance), and their quantum yield rarely exceeds 0.1%.[20] Therefore, studies have centered on enhancing the performance of AuNCs and explaining the mechanism of their luminescence. It has been reported that the luminescence of

Received: February 9, 2021
Accepted: April 27, 2021
Published: May 6, 2021

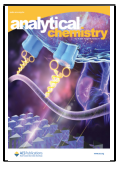

https://doi.org/10.1021/acs.analchem.1c00616
Anal. Chem. 2021, 93, 7275−7282

AuNCs is strongly linked to the restriction of intramolecular movement (RIM).[21] The intramolecular movement of AuNCs can open their nonradiative transition channels, thereby attenuating the fluorescence properties of AuNCs and showing aggregation-induced emission (AIE) properties. Hence, it is an efficient approach to improve the fluorescence performance of AuNCs by restraining intramolecular movement. For instance, Xie's team exploited organic solvents, metal cations, and other methods to limit the intramolecular movement of AuNCs, which turned on the AIE properties and improved the fluorescence performance.[22,23]

As a typical representative of metal organic frameworks (MOFs), zeolite-like imidazole framework structure materials (ZIFs) have been used in sensors, catalysis and gas storage due to the microporosity, biodegradability and specific surface area.[24−27] Especially, various nanomaterials can be embedded in the aperture of ZIFs, which can not only exhibit the unique porosity of the ZIFs, but also take into account the characteristics of magnetism and fluorescence.[28−30] For example, Hu et al. incorporated CuNCs into ZIF-8 to form CuNCs/ZIF-8 for the sensitive detection of H_2O_2,[31] while Fan et al. packaged AgNCs into ZIF-8 to detect Cu^{2+} in blood.[32] After doping CuNCs or AgNCs into ZIF-8, both the quantum yield and fluorescence lifetime was improved. Therefore, it is feasible to encapsulate metal nanoclusters in ZIF-8 for the improvement of the stability and fluorescence performance.

Due to the convenient screen operability, imaging performance, and powerful data processing, smartphones have gradually developed into comprehensive tools for receiving, processing, and displaying data. Through various sensors in the smart phone or additional sensor accessories, it can transmit light, sound, heat, and other signals for biochemical substance detection.[33−35] Guan et al. used an electrochemical analyzer controlled by a smartphone to achieve the detection of microcystin-LR,[36] while Amirjani et al. used a smartphone to extract the RGB value of an image to realize the analysis of ammonia,[37] suggesting that the smartphone has opened up a new field for the testing of biochemical or chemical substances.

In this work, fluorescence and colorimetric methods were married to detect OPs on the basis of a AuNCs@ZIF-8 composite. In Scheme 1, ZIF-8@AuNCs were synthesized *in situ* by AuNCs and ZIF-8 precursors. Since ZIF-8 restricted the movement of AuNCs, attenuated the nonradiative decay, and turned on the radiation channel, AuNCs@ZIF-8 can emit strong fluorescence. The combination of acetylcholinesterase (AChE) and choline oxidase (CHO) can enzymatically hydrolyze acetylcholine (ACh) to generate H_2O_2, which can destroy the structure of ZIF-8 and reduce the fluorescence of AuNCs@ZIF-8, while AuNCs showed a certain peroxidase activity to transform colorless TMB to blue oxTMB. Due to the inhibition of AChE activity by OPs, a fluorescence−colorimetric dual-signal detection of OPs was achieved by monitoring the fluorescence change of AuNCs@ZIF-8 and also the color change of TMB. In particular, colorimetric paper strips were prepared for the visible detection of OPs, while a smartphone platform was further explored to recognize the gray value of the solution color for the quantitative detection of OPs.

Scheme 1. Schematic Diagram of the Mechanism for the Detection of OPs

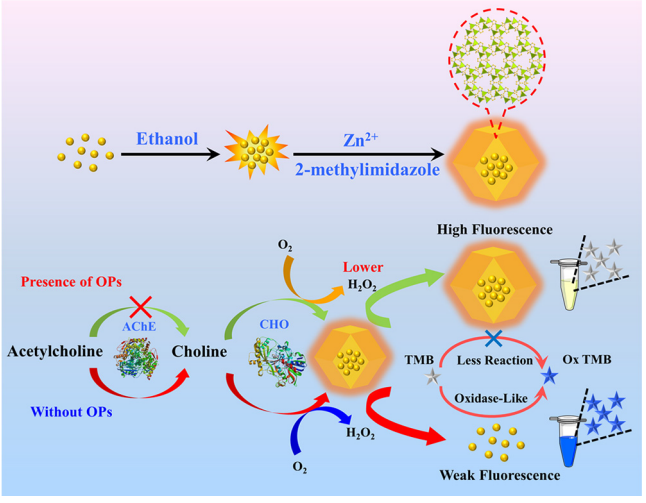

2. EXPERIMENTAL SECTION

2.1. Reagents and Instruments. 3,3′,5,5′-Tetramethylbenzidine (TMB), $Zn(NO_3)_2{\cdot}6H_2O$, glutathione (GSH), and 2-methylimidazole were obtained from Aladdin Biological Technology Co. Ltd., Beijing. $HAuCl_4$ was purchased from Shenyang Jinke reagent factory. Choline oxidase (CHO) was purchased from Sigma-Aldrich. Acetylcholinechloride (ACh) and acetylcholinesterase (AChE) were supplied by Macklin Biochemical Technology Co., Ltd., Shanghai. Acephate, cyantraniliprole, spirotetramat, thiamethoxam, tebuconazole, hymexazol, glyphosate, malathion, parathion, pirimiphos-methyl and fenitrothion were acquired from Dr. Zhenlin Xu and Jinliang Jia, South China Agricultural University. The above pesticides were all analytical reagents. Except for acephate and glyphosate dissolved in water, all other pesticides were dissolved in DMSO.

Transmission electron microscopy (TEM, Talos L120C, Thermo Fisher, USA) and scanning electron microscopy (SEM, Talos F200S, Thermo Fisher, USA) were used to observe the morphology of materials, while X-ray powder diffractometry (XRD, Rigaku-Ultima IV, Japan) and X-ray photoelectron spectroscopy (XPS, Thermo fisher, USA) were used to detect the crystal structures and the elements of materials. The N_2 adsorption/desorption and the pore size distribution were investigated by an automatic specific surface area and pore size distribution analyzer (Gemini VII 2390, Micromeritics, USA). The content of Au in the material was quantified by inductively coupled plasma−atomic emission spectrometry (ICP-AES, 720ES, Agilent, USA). A UV−vis spectrophotometer (UV2550, Shimadzu, Japan) was used to record the absorption spectra. An F-7000 instrument (Hitachi, Japan) was used to record the fluorescence spectra, and an FLS-980 fluorescence spectrometer (Edinburgh, England) was used to record the fluorescence lifetime and quantum yield, respectively.

2.2. Synthesis of AuNCs. According to a previous method, AuNCs were synthesized by using GSH as a stabilizer and reducing reagent.[38] In detail, all glass instruments were soaked and cleaned with aqua regia before use. With stirring at room temperature, an $HAuCl_4$ solution (7.5 mL, 4 mM) was added to a GSH solution (7.5 mL, 6 mM) and mixed for 5 min, followed by heating at 70 °C for 12 h under dark conditions. After dialysis for 24 h, the yellow AuNCs solution was stored at 4 °C for further use.

https://doi.org/10.1021/acs.analchem.1c00616
Anal. Chem. 2021, 93, 7275−7282

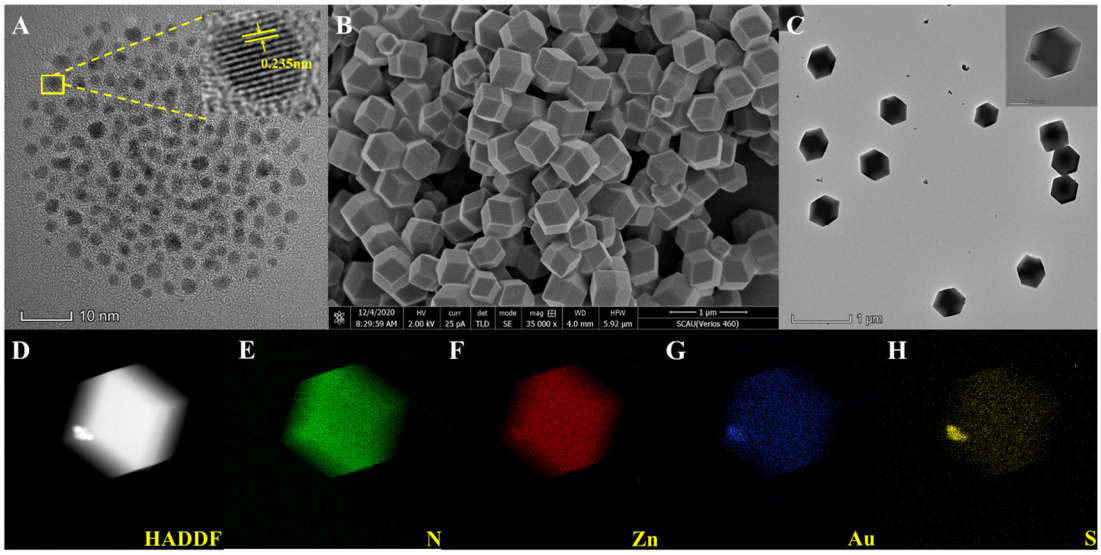

Figure 1. TEM and HRTEM images of (A) AuNCs in water. (B) SEM and (C) TEM images of AuNCs@ZIF-8. (D−H) HAADF-STEM image and elemental mappings of N, Zn, Au, and S, respectively.

2.3. Preparation of AuNCs@ZIF-8. First, 3 mL of ethanol was added to 4 mL of an AuNCs solution and mixed uniformly. After centrifugation at 11000 rpm for 15 min, the precipitated AuNCs were redispersed in 2 mL of methanol. Subsequently, the AuNCs−methanol solution and $Zn(NO_3)_2$−methanol solution (30 mM, 10 mL) were mixed and stirred for 5 min, followed by the addition of a 2-methylimidazole−methanol solution (90 mM, 10 mL). After the mixture was ultrasonically dispersed for 40 min at room temperature, the product was gathered by centrifuging, washing with methanol, and drying under vacuum overnight.

2.4. Fabrication of the Marriage of Fluorescence and Colorimetric Biosensor. For the fluorescence detection, AuNCs@ZIF-8 (5 mg/mL, 100 μL) was mixed with 695 μL of H_2O. At the same time, 15 μL of acephate solutions of different concentrations and 15 μL of AChE (0.4 U/mL) were incubated in PBS (pH 7.4) for 15 min, and 160 μL of 0.5 M ACh was further added for incubation. Then, 15 μL of CHO (0.4 U/mL) was added and incubated for another 15 min to prepare the AChE−OPs−ACh−CHO solution. After this solution was mixed with the AuNCs@ZIF-8 solution and incubated for 30 min, the fluorescence spectrum was recorded between 450 and 700 nm.

For the colorimetric detection, 100 μL of ZIF-8@AuNCs (5 mg/mL) was mixed with 665 μL of NaAc−HAc buffer (pH 4), followed by addition of 30 μL of a TMB solution (30 mM). After the mixture was incubated with a AChE−OPs−ACh−CHO solution for 15 min, the UV−vis absorption spectrum was measured from 500 to 800 nm.

3. RESULTS AND DISCUSSION

3.1. Characterization of AuNCs@ZIF-8. AuNCs were synthesized by using GSH as a stabilizer and reducing reagent and characterized by TEM. As shown in Figure 1A, AuNCs had a quasi-spherical structure with a uniform size distribution, and the average size was about 2 nm. The HRTEM image (inset in Figure 1A) showed an individual AuNC with a lattice spacing of 0.235 nm, which corresponded to the (111) crystal plane of Au. In addition, when AuNCs were dispersed in 50% ethanol, due to solvent-induced effects, significant aggregation was discovered and the size of the AuNCs increased to 60 nm (Figure S1).[22] After AuNCs were encapsulated into ZIF-8, their shape and size were not significantly different from those of pure ZIF-8,[39] showing a rhombic dodecahedral shape (Figure 1B). AuNCs@ZIF-8 was synthesized through the coordination of Zn^{2+} with the carboxyl group on the GSH ligand of AuNCs and the N atom in 2-methylimidazole during the formation of ZIF-8; thus, ZIF-8 could be self-assembled around the AuNCs.[20] Moreover, it is worth noting that by adjusting the dosage of AuNCs (from 1 to 4 mL), the morphology and size of the rhombic dodecahedron of ZIF-8@AuNCs remained stable. However, when the amount of AuNCs was increased to 5 mL, obvious aggregation and incomplete encapsulation could be found (Figure S2).

Interestingly, after the amount of AuNCs was fixed, an increase in the reaction time in 10−40 min increased the fluorescence intensity gradually, which can be attributed to the AIE effect of AuNCs. In detail, AuNCs were encapsulated in ZIF-8 after aggregation in methanol solvent. The rotation and vibration of AuNCs were further restricted by coordination bonds, which enhanced the AIE effect and fluorescence intensity of AuNCs. However, when the reaction time was over 40 min, the size of ZIF-8@AuNCs increased, but the fluorescence intensity decreased (Figure S3). A longer reaction time caused a larger size of ZIF-8, which increased the thickness of ZIF-8 to block the transmission of light and the excitation of AuNCs.

Since the ZIF-8 shell has a certain thickness and the size of AuNCs is small, it is difficult to observe the existence of AuNCs by TEM. Energy dispersive spectroscopic (EDS) mapping was performed through HAADF-STEM. The elements N, Zn, Au, and S could be clearly found, confirming the embedding of AuNCs in ZIF-8 (Figure 1E−H). As in Figure 2A, the XRD result substantiated the formation of ZIF-8 in AuNCs@ZIF-8, basically consistent with the spectrum of pure ZIF-8, which suggested that the packaging of AuNCs did not affect the crystal growth of ZIF-8. However, the obvious diffraction peaks of Au could not be observed in the XRD spectrum, which may be caused by the low amount and poor

https://doi.org/10.1021/acs.analchem.1c00616
Anal. Chem. 2021, 93, 7275−7282

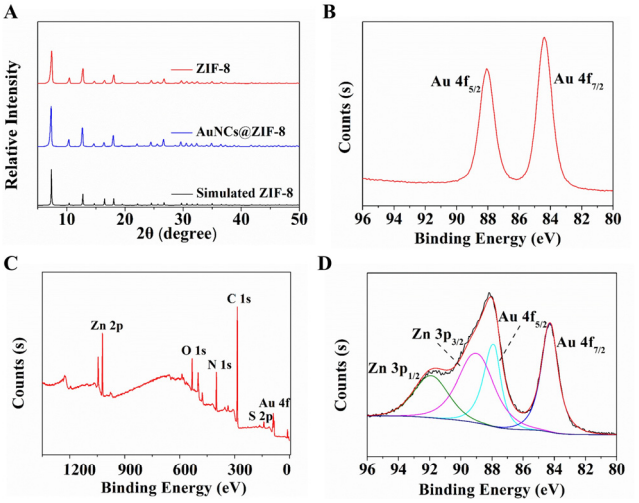

Figure 2. (A) XRD characterization of ZIF-8 (red line), AuNCs@ZIF-8 (blue line), and simulated ZIF-8 (black line). (B) XPS analysis of Au 4f for AuNCs. (C) XPS survey of AuNCs@ZIF-8. (D) XPS analysis of Au 4f and Zn 3p for AuNCs@ZIF-8.

crystallinity of AuNCs. The specific content of Au was still detected as 1.86% by ICP-AES.

In addition, XPS experiments were performed to investigate the charge state of the Au element. It is obvious that AuNCs@ZIF-8 contains Au, S, O, C, N, and Zn elements (Figure 2C). In Figure 2B, Au 4f of AuNCs had two peaks at 88.0 and 84.3 eV, corresponding to Au $4f_{5/2}$ and Au $4f_{7/2}$, respectively. In AuNCs@ZIF-8, there was no significant difference between the positions of Au $4f_{5/2}$ and Au $4f_{7/2}$ (Figure 2D), but the fluorescence intensity was significantly improved. The XPS results indicated that the increase in fluorescence was not caused by the change in the charge state of Au but was due to the aggregation of AuNCs and the confinement effect of ZIF-8.

Furthermore, the porous property of AuNCs@ZIF-8 was analyzed by N_2 adsorption isotherms and a pore size distribution curve. As shown in Figure S4, AuNCs@ZIF-8 exhibited a type I isotherm property. Due to the micropores, it exhibited an extremely strong adsorption capacity under low relative pressure. The average pore diameter and BET surface area of ZIF-8 were 1.437 nm and 1793.71 m^2/g, respectively. In contrast, AuNCs@ZIF-8 had isothermal characteristics and porous structure similar to those of pure ZIF-8 (pore size 1.413 nm, BET surface area 1758.75 m^2/g). With the encapsulation of AuNCs, the pore diameter and surface area of AuNCs@ZIF-8 were slightly reduced, but the porous structure of ZIF-8 remained, which further proved that instead of being embedded in the holes of ZIF-8, AuNCs were encapsulated in ZIF-8.

In order to study whether ZIF-8 can effectively improve the fluorescence performance of AuNCs, the fluorescence abilities of AuNCs and AuNCs@ZIF-8 were compared. For AuNCs, we had discovered AuNCs had an aggregation-induced emission effect,[40] where AuNCs can be agglomerated by a solvent-induced effect and the fluorescence intensity can be increased. In Figure S5, the intensity of the AuNCs solution was about 400, and a poor orange light emission under ultraviolet light was found. In contrast, the intensity of AuNCs@ZIF-8 was approximately 4 times that of AuNCs, and the emitted fluorescence changed from orange to yellow, which was consistent with the small blue shift of the fluorescence spectrum. In addition, as illustrated in Figure S6, the fluorescence lifetime and quantum yield of AuNCs@ZIF-8 were 6.83 μs and 4.63%, respectively, which were higher than those of AuNCs (fluorescence lifetime 3.99 μs, quantum yield 0.28%). Moreover, the fluorescence intensity of AuNCs@ZIF-8 showed negligible fluctuations even when it was exposed to excitation at 365 nm for 3 h (Figure S7), indicating that it had favorable stability. The restriction of intramolecular motion enhanced the fluorescence of AuNCs, and this was further verified, as shown in Video S1. When the AuNCs solution was frozen by fluid nitrogen, a bright orange fluorescence emission was observed. As the time lapsed, the temperature increased and the intensity decreased gradually and eventually returned to the original weak emission state. In the frozen state, the movement of AuNCs was effectively restricted; thereby the nonradiative relaxation path was inhibited and hence AuNCs emitted bright fluorescence. After thawing, the molecular motion was restored, and the nonradiative relaxation path was opened, resulting in a gradual decrease in fluorescence. When AuNCs were encapsulated into ZIF-8, the rotation and vibration of AuNCs were restricted by coordination bonds, and the confined space of ZIF-8 might reduce the free movement of AuNCs. Accordingly, the relaxation paths of the excited AuNCs were limited and electrons could return to the ground state through radiative transitions instead of nonradiative transitions. Therefore, ZIF-8 can effectively improve the fluorescence performance of AuNCs.

3.2. Mechanism of Dual-Mode Fluorescence and Colorimetric Sensors. Scheme 1 is a representative diagram of the marriage of fluorescence and colorimetric biosensors for detecting OPs. Specifically, after AuNCs were encapsulated in ZIF-8, Zn^{2+} could form a coordinate bond with the carboxyl group on the GSH ligand of AuNCs. In addition, the limited space of ZIF-8 increased the association of Au atoms with the surface groups of AuNCs, leading to the accumulation of AuNCs.[41] In addition, Zn^{2+} also played an important role during the *in situ* synthesis of ZIF-8. Consequently, the aggregated AuNCs were wrapped by ZIF-8; thus, the vibration and rotation of AuNCs were suppressed and the nonradiative transition of AuNCs was avoided, achieving an enhancement of the fluorescence signal.[42]

In the fluorescence detection, H_2O_2 can destroy the structure of ZIF-8,[43] weaken its restraint on AuNCs, and decrease the fluorescence. In Figure S8, after incubation in H_2O_2 for a period of time, the fluorescence intensity of AuNCs@ZIF-8 decreased sharply, and finally it was similar to that of pure AuNCs. A TEM analysis was further carried out to explore the quenching mechanism by H_2O_2. As shown in Figure S9, after AuNCs@ZIF-8 reacted in 3% H_2O_2 for a certain period of time, the rhombic dodecahedral structure of ZIF-8 was broken. Since the 2-methylimidazole ligand of ZIF-8 has antioxidant activity, it can react with oxidants such as H_2O_2 to destroy the structure of ZIF-8.[43] Thus, the restraining effect on AuNCs disappeared, the free movement of AuNCs was restored, and the fluorescence decreased. In addition, AChE can enzymatically hydrolyze acetylcholine to produce choline, which can produce H_2O_2 under the action of choline oxidase. Moreover, OPs can inhibit the activity of AChE, causing a decrease in the production of H_2O_2, a weakening of the decomposition of ZIF-8, and a gradual recovery of fluorescence; thus, a "turn-on" fluorescence mode was achieved.

https://doi.org/10.1021/acs.analchem.1c00616
Anal. Chem. 2021, 93, 7275−7282

In a colorimetric detection, AuNCs have been reported to exhibit peroxidase mimic activity.[44,45] Au elements in AuNCs usually exist in the form of Au(0) and Au(I). After H_2O_2 was adsorbed by AuNCs, the O−O bond in H_2O_2 could be decomposed by Au(0) or Au(I) in AuNCs to generate hydroxyl radicals ($^{\bullet}OH$), thereby turning TMB blue.[44,45] Different concentrations of OPs can cause different inhibitory effects on AChE; thus, a color change from blue to colorless can be discovered. Therefore, a colorimetric detection by the naked eye can be obtained, and a quantitative detection can be also achieved by measuring the absorbance change.

3.3. Optimization of Detection Conditions. The influence of factors such as ACh volume, AChE concentration, CHO concentration, pH, and incubation time was investigated. The concentration of ACh is of great significance to the final enzymatic hydrolysis product, H_2O_2. In Figure S10A, as the ACh volume was increased, the fluorescence intensity decreased significantly. When the volume of ACh exceeded 160 μL, the fluorescence change was not obvious, indicating that the optimal volume of ACh was 160 μL. Figure S10B,C shows that, as the concentration of AChE and CHO was increased, the fluorescence gradually decreased. Due to the limited amount of substrate, after the concentration exceeded 0.4 U/mL, the substrate was completely hydrolyzed, and subsequent changes were not prominent. Therefore, the optimal concentrations of both AChE and CHO were selected as 0.4 U/mL. In the pH range of 2−7, with an increase in pH, the enzyme activity of AChE and CHO gradually increased, and the fluorescence change also increased. However, when pH was over 8, the fluorescence change decreased due to the denaturation of enzymes and the decomposition of OPs in the overly alkaline environment. These changes indicate that the optimal pH was 7.4 (Figure S10D). Furthermore, the inhibition degree was relative to the incubation time. When the time was lower than 15 min, the inhibition degree of AChE by OPs gradually increased and the amount of choline gradually decreased; thus, the amount of final H_2O_2 decreased and the corresponding fluorescence was gradually enhanced. However, the fluorescence displayed no significant change with a further increase in the incubation time (Figure S10E); thus, 15 min was selected as the optimum time.

3.4. Performance of the Marriage of Fluorescence and Colorimetric Sensors. Under the optimal conditions, the developed dual-mode fluorescence−colorimetric sensor was used to detect OPs on the basis of the inhibitory effect of OPs on AChE. Here, acephate was used as a representative of OPs. For the fluorescence detection, AChE can enzymatically hydrolyze ACh to produce choline. Choline was hydrolyzed by CHO, and the product, H_2O_2, can decompose ZIF-8, thereby producing the greatest fluorescence quenching effect. As shown in Figure 3A,B, by an increase in different concentrations of OPs to inhibit AChE, the amount of H_2O_2 decreased with an increased concentration of OPs, and the decomposition degree of ZIF-8 was weakened, resulting in an increase in fluorescence intensity (I). In the range from 0.75 μg/L to 75 mg/L, a linear relationship was obtained between I and the logarithm of the OPs concentration as $I = 255.34 \log C + 1243.31$ ($R^2 = 0.996$, S/N = 3), while the detection limit was 0.67 μg/L.

Simultaneously, a colorimetric detection was performed by recording the peak intensity of the produced blue oxTMB. With the aid of ACh, AChE and CHO can promote the formation of H_2O_2. It is worth mentioning that AuNCs have

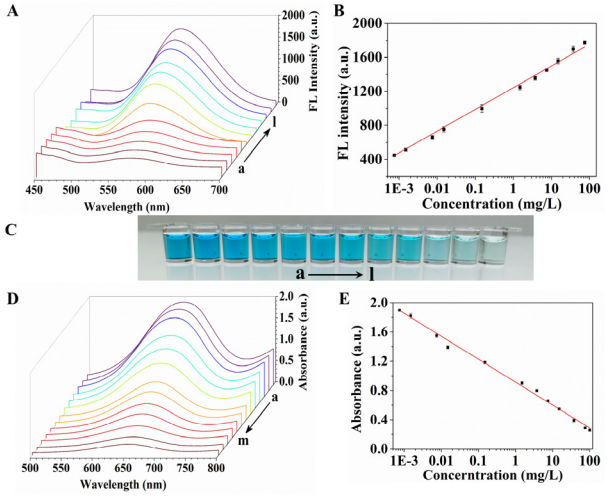

Figure 3. (A) Fluorescence spectra at different acephate concentrations (λ_{ex} = 365 nm) and (B) the calibration. Concentrations from a to l: 0, 0.00075, 0.0015, 0.075, 0.015, 0.15, 1.5, 3.75, 7.5, 15, 37.5, 75 mg/L. (C) Photographs at different concentrations of OPs. Concentrations from a to l: 0, 0.00075, 0.0015, 0.075, 0.015, 0.15, 1.5, 3.75, 7.5, 15, 37.5, 75 mg/L. (D) UV−vis spectra at different acephate concentrations and (E) the calibration. Concentrations from a to m: 0, 0.00075, 0.0015, 0.075, 0.015, 0.15, 1.5, 3.75, 7.5, 15, 37.5, 75, 100 mg/L.

peroxidase-like activity, thus H_2O_2 can activate AuNCs to catalyze the oxidation of TMB and form a blue color. When AChE was incubated with OPs, its activity was inhibited and less H_2O_2 was produced, which weakened the catalytic oxidation of TMB and the blue color decreased (Figure 3C,D). As shown in Figure 3E, the calibration showed a good linear relationship between the absorbance value (A) at 655 nm and the logarithm of the OPs concentration can be found as $A = -0.32 \log C + 0.91$ (R^2 = 995, S/N = 3) in the range of 0.75 μg/L to 100 mg/L, and the detection limit was 0.3 μg/L. Moreover, Table S1 summarizes some comparisons for the determination of OPs based on different fluorescent materials, demonstrating that the unique advantages of dual-mode signal detection achieved a sensitive analysis.

To investigate the response to other OPs, glyphosate, malathion, parathion, pirimiphos-methyl, and fenitrothion were analyzed. In Figure 4A, this biosensor was used to detect different OPs at the same concentration, showing that the signals were slightly different (the individual ranges are shown in Table S2). The inhibition of AChE enzyme activity can be inhibited by different OPs, which indicated that the dual-mode biosensor was suitable for OPs detection. Simultaneously, the selectivity was also investigated by detecting several commercial non-OPs pesticides including thiamethoxam, cyantraniliprole, spirotetramat, tebuconazole, and hymexazol (the structural formulas are shown in Figure S11). Only in the presence of OPs did the fluorescence signal have an obvious response, and the color signal was different from that of other pesticides (Figure 4B,C). Thus, the change in fluorescence and color was caused by the inhibitory effect of OPs on AChE, implying that this fluorescence−colorimetric biosensor exhibited good selectivity.

To evaluate the application potential and feasibility in actual detection, the standard addition method was used for monitoring different OPs levels in water samples and lettuce extract. By a simple centrifugation of the sample to remove

https://doi.org/10.1021/acs.analchem.1c00616
Anal. Chem. 2021, 93, 7275−7282

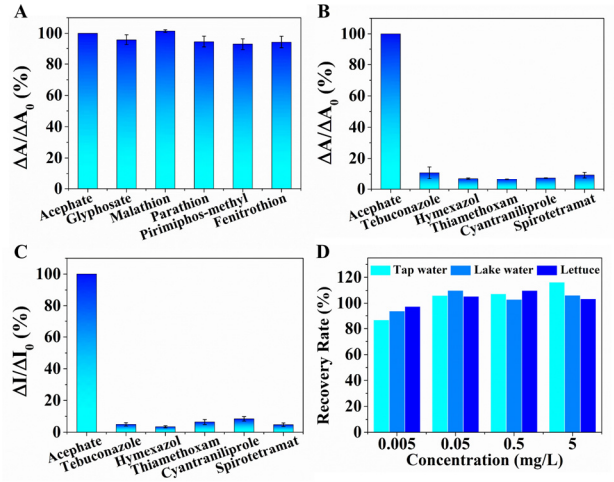

Figure 4. (A) Absorbance change of 15 mg/L of different OPs to the sensing system. Selectivity of the biosensor by UV−vis (B) and fluorescence (C) detection. (D) Recovery test in a water sample.

insoluble impurities, a series of 5, 0.5, 0.05, and 0.005 mg/L OPs samples were added. As shown in Figure 4D and Table S3, the recoveries were between 86.0% and 116.4%, indicating that this biosensor can be applied in actual samples.

3.5. Test Strips and Smartphone Platform for the Detection of OPs. Due to the necessity of on-site testing, portable equipment should be also considered. First, a colorimetric test paper for OPs detection was made. As shown in Figure 5, there is no obvious difference between the

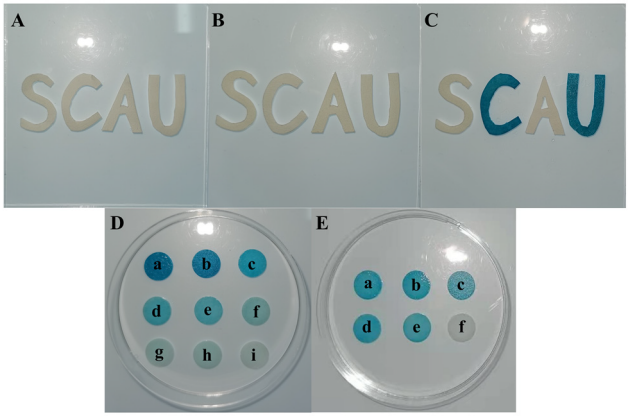

Figure 5. (A) General filter paper tailored with "SCAU". (B) The filter paper in (A) was dyed with AuNCs@ZIF-8 in NaAc-HAc buffer (pH 4) with 50 μL of TMB (30 mM). (C) Spray of "C" and "U" with 1% H_2O_2. (D) Photographs of paper-based biosensors responding to different concentrations of OPs (from a to i: 0, 0.00075, 0.0015, 0.015, 0.15, 1.5, 7.5, 15, 30 mg/L). (E) Photographs of paper-based biosensors responding to different pesticides (from a to f: thiamethoxam, cyantraniliprole, spirotetramat, tebuconazole, hymexazol, and acephate).

filter paper before (Figure 5A) and after (Figure 5B) the AuNCs@ZIF-8-TMB-buffer impregnation. However, after exposure to 1% H_2O_2, the filter paper turned blue (Figure 5C). Moreover, after incubation of different concentrations of OPs (from a to i: 0, 0.00075, 0.0015, 0.015, 0.15, 1.5, 7.5, 15, 30 mg/L) with AChE and further addition of the mixed solution, the blue degree of the test paper decreased significantly with an increase in OPs concentration (Figure 5D). The color change of the test paper was visible to the naked eye. In addition, the response of the test strip to various pesticides was also evaluated. As anticipated, other types of pesticides can turn the test strip blue, but OPs cannot, which demonstrated that the test strip had a good selectivity for OPs. Therefore, the developed method may be used in the visual detection of OPs.

To further realize the quantitative detection of OPs, a smartphone APP (Sensor Photo) was used to identify the gray value of the colorimetric sensor (Figure 6). Significantly, the

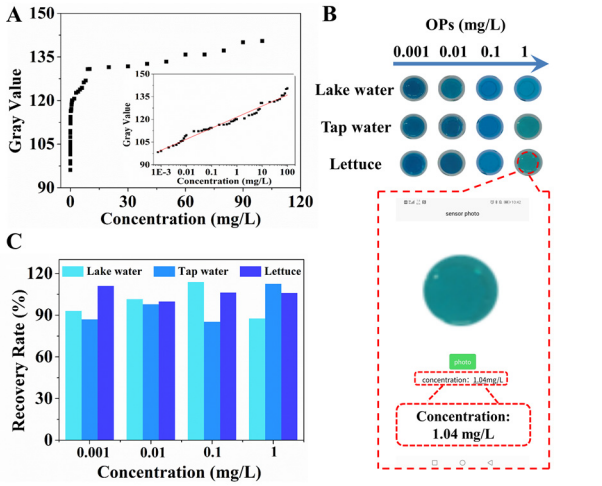

Figure 6. (A) Relationship of gray values of solutions and concentration of OPs. (B) Application of the colorimetric sensor to real samples. Inset: a smartphone recognizes the concentration of OPs in the solution. (C) Recovery test in real samples by the smartphone APP.

process of photographing and recognizing gray values needs to be performed on a smartphone. When 0.00075−100 mg/L of OPs were added, the biosensor showed a color variance from blue to colorless. Then, the average color of each solution was read out by Python. In order to simplify the analysis, we converted the color value to a gray value before data analysis. It turned out that the gray value of the solution was closely related to the logarithm of the OPs concentration, and the linear equation was $G = 7.35 \log C + 121.51$ ($R^2 = 0.974$) with a detection limit of 0.4 μg/L. On the basis of the relationship between the gray value and the concentration of OPs, a smartphone APP (Sensor Photo) was developed using Python (the main interface and usage of APP are shown in Figure S12, and the installation program for the APP is given in the Supporting Information). Moreover, the availability of a smartphone APP for OPs analysis in practical samples was investigated by adding acephate with different concentrations to lettuce extract and water samples (Figure 6B). The gray values of the solution were confirmed by the smartphone APP, and the recoveries of OPs ranged from 85.2% to 113.8% through calculations (Figure 6C). This was an indication that the combination of this method with a smartphone can be portable and real-time quantitative detection of OPs in real samples such as lettuce extract and water sample can be achieved for the detection OPs by the naked eye with an equipment-free pattern. In addition, the detection results with HPLC/MS and this method were compared. The ESI-MS/MS detection parameters of acephate are shown in Table S4. The results are shown in Table S5, implying that acephate in a

https://doi.org/10.1021/acs.analchem.1c00616
Anal. Chem. 2021, 93, 7275−7282

sample with 5.0 μg/L was determined as 4.3 μg/L by HPLC/MS and 4.1 μg/L by this method. The concentrations of the samples with 0.015, 0.15, and 1 mg/L were identified as 0.016, 0.15, and 0.99 mg/L by HPLC/MS and 0.017, 0.14, and 1.06 mg/L by this method, respectively. This showed that the constructed sensor has good detection performance.

4. CONCLUSIONS

In summary, we successfully packaged AuNCs into ZIF-8, which enabled an AIE effect of AuNCs and improved their fluorescence performance. The marriage of a fluorescence and colorimetric sensor was constructed for the detection of OPs. In comparison with a traditional single-signal biosensor, this method was more sensitive and reliable, which can be ascribed to the following reasons. (1) By encapsulation of AuNCs with an AIE effect into ZIF-8, the molecular movement was restricted and the fluorescence signal was amplified. (2) With the kernel concept of inhibiting the enzymatic hydrolysis product, H_2O_2, by the decomposition effect of H_2O_2 on ZIF-8 and the peroxidase mimic activity of AuNCs, fluorescence and color changes were generated, thereby achieving dual signal detection. In particular, a colorimetric test paper was developed to realize the visual detection of OPs. In addition, the gray values of the solution were acquired from a smartphone APP for an on-site quantitative detection of OPs with a detection limit of 0.4 μg/L. Therefore, this sensing method has potential to detect OPs in the environment, providing a convenient and reliable method for environmental safety.

■ ASSOCIATED CONTENT

Supporting Information

The Supporting Information is available free of charge at https://pubs.acs.org/doi/10.1021/acs.analchem.1c00616.

Parameters of HPLC/MS, TEM image of AuNCs in 50% ethanol, fluorescence spectrum and TEM image of ZIF-8@AuNCs synthesized with different volumes of gold clusters, TEM images of ZIF-8@AuNCs at different reaction times, N_2 adsorption/desorption isotherms and pore diameter distributions of ZIF-8 and ZIF-8@AuNCs, fluorescence spectra of AuNCs and ZIF-8@AuNCs and corresponding photos under a 365 nm UV lamp, time-resolved emission decay curves of the AuNCs and ZIF-8@AuNCs, TEM images of ZIF-8@AuNCs and ZIF-8@AuNCs after incubation in aqueous solution with H_2O_2, influence factors, main interface of the smartphone APP, analytical performances of various methods for OPs detection, individual ranges of the various OPs, and concentrations of acephate in samples by HPLC/MS and APP (PDF)

Fluorescence image of AuNCs aqueous solution after it was frozen with liquid nitrogen and gradually warmed to room temperature (MP4)

Installation program for the APP sensor photo.apk (ZIP)

■ AUTHOR INFORMATION

Corresponding Authors

Aori Qileng − *Key Laboratory for Biobased Materials and Energy of Ministry of Education, College of Materials and Energy and The Guangdong Provincial Key Laboratory of Food Quality and Safety, College of Food Science, South China Agricultural University, Guangzhou 510642, People's Republic of China*; Email: arql@stu.scau.edu.cn

Kangshun Li − *College of Mathematics and Informatics, South China Agricultural University, Guangzhou 510642, People's Republic of China*; Email: likangshun@scau.edu.cn

Yingju Liu − *Key Laboratory for Biobased Materials and Energy of Ministry of Education, College of Materials and Energy and The Guangdong Provincial Key Laboratory of Food Quality and Safety, College of Food Science, South China Agricultural University, Guangzhou 510642, People's Republic of China*; orcid.org/0000-0002-1130-4945; Email: liuyingju@hotmail.com

Authors

Yue Cai − *Key Laboratory for Biobased Materials and Energy of Ministry of Education, College of Materials and Energy, South China Agricultural University, Guangzhou 510642, People's Republic of China*

Hongshuai Zhu − *Key Laboratory for Biobased Materials and Energy of Ministry of Education, College of Materials and Energy and The Guangdong Provincial Key Laboratory of Food Quality and Safety, College of Food Science, South China Agricultural University, Guangzhou 510642, People's Republic of China*

Weichi Zhou − *College of Mathematics and Informatics, South China Agricultural University, Guangzhou 510642, People's Republic of China*

Ziyin Qiu − *Key Laboratory for Biobased Materials and Energy of Ministry of Education, College of Materials and Energy, South China Agricultural University, Guangzhou 510642, People's Republic of China*

Congcong Chen − *Key Laboratory for Biobased Materials and Energy of Ministry of Education, College of Materials and Energy, South China Agricultural University, Guangzhou 510642, People's Republic of China*

Complete contact information is available at: https://pubs.acs.org/10.1021/acs.analchem.1c00616

Author Contributions

‖Y.C. and H.Z. contributed equally to the work.

Notes

The authors declare no competing financial interest.

■ ACKNOWLEDGMENTS

This work was supported by the National Natural Science Foundation of China (21874048), the Key R & D Program of Guangdong Province (2019B020219003), the Science and Technology Planning Project of Guangdong Province (2020B1212060059), the National Key Research and Development Program of China (SQ2017YFC160089), and the Educational Commission Foundation of Guangdong Province (2020ZDZX2025).

■ REFERENCES

(1) Wang, J.; Duan, H. L.; Fan, L.; Zhang, J.; Zhang, Z. Q. *Food Chem.* **2021**, *338*, 127805.

(2) Fahimi-Kashani, N.; Hormozi-Nezhad, M. R. *Sens. Actuators B - Chem* **2020**, *322*, 128580.

(3) Ma, R. X.; Xu, M.; Liu, C.; Shi, G. Y.; Deng, J. J.; Zhou, T. S. *ACS Appl. Mater. Interfaces* **2020**, *12*, 42119−42128.

(4) Qin, Y.; Wu, Y.; Chen, G. J.; Jiao, L.; Hu, L. Y.; Gu, W. L.; Zhu, C. Z. *Anal. Chim. Acta* **2020**, *1130*, 100−106.

(5) Qiu, F.; Liu, J.; Zhang, H. T.; Li, H. Y.; Liu, J. H.; Shi, X. S.; Li, C. L.; Shi, Y. J.; Hu, Y.; Guo, Y. L.; Gao, X. K.; Ai, S. Y.; Jiang, L. *Adv. Electron. Mater.* **2020**, *6*, 2000579.
(6) Kan, H. S.; Wang, T. C.; Yu, J. X.; Qu, G. Z.; Zhang, P.; Jia, H. Z.; Sun, H. W. *J. Hazard. Mater.* **2021**, *401*, 123361.
(7) Yao, T. T.; Liu, A. R.; Liu, Y.; Wei, M.; Wei, W.; Liu, S. Q. *Biosens. Bioelectron.* **2019**, *145*, 111705.
(8) Lu, T. Y.; Zhan, S. N.; Zhou, Y. F.; Chen, X. R.; Huang, X. L.; Leng, Y. K.; Xiong, Y. H.; Xu, Y. *Anal. Methods* **2018**, *10*, 5797−5802.
(9) Zhang, Y. Q.; Xu, Z. L.; Wang, F.; Cai, J.; Dong, J. X.; Zhang, J. R.; Si, R.; Wang, C. L.; Wang, Y.; Shen, Y. D.; Sun, Y. M.; Wang, H. *Anal. Chem.* **2018**, *90*, 12886−12892.
(10) Zhang, N.; Gao, J.; Huang, C. H.; Liu, W.; Tong, P.; Zhang, L. *Anal. Chim. Acta* **2016**, *934*, 122−131.
(11) Harshit, D.; Charmy, K.; Nrupesh, P. *Food Chem.* **2017**, *230*, 448−453.
(12) Yao, J.; Liu, Z.; Jin, M.; Zou, Y.; Chen, J.; Xie, P.; Wang, X.; Akinoglu, E. M.; Zhou, G.; Shui, L. *Sens. Actuators B - Chem* **2020**, *321*, 128517.
(13) Tian, X.; Liu, L.; Li, Y.; Yang, C.; Zhou, Z.; Nie, Y.; Wang, Y. *Sens. Actuators B - Chem*, **2018**, *256*, 135−142.
(14) Yan, X.; Song, Y.; Zhu, C.; Li, H.; Du, D.; Su, X.; Lin, Y. *Anal. Chem.* **2018**, *90* (4), 2618−2624.
(15) Huang, S.; Guo, M.; Tan, J.; Geng, Y.; Wu, J.; Tang, Y.; Su, C.; Lin, C. C.; Liang, Y. *ACS Appl. Mater. Interfaces* **2018**, *10*, 39056−39063.
(16) Xu, X. Y.; Yan, B.; Lian, X. *Nanoscale* **2018**, *10*, 13722−13729.
(17) Ding, C.; Xu, Y.; Zhao, Y.; Zhong, H.; Luo, X. *ACS Appl. Mater. Interfaces* **2018**, *10*, 8947−8954.
(18) You, J. G.; Lu, C. Y.; Kumar, A. S.K; Tseng, W. L. *Nanoscale* **2018**, *10*, 17691−17698.
(19) Venkatesh, V.; Shukla, A.; Sivakumar, S.; Verma, S. *ACS Appl. Mater. Interfaces* **2014**, *6*, 2185−2191.
(20) Cao, F. F.; Ju, E. G.; Liu, C. Q.; Li, W.; Zhang, Y.; Dong, K.; Liu, Z.; Ren, J. S.; Qu, X. G. *Nanoscale* **2017**, *9*, 4128−4134.
(21) Tian, R.; Zhang, S.; Li, M.; Zhou, Y.; Lu, B.; Yan, D.; Wei, M.; Evans, D. G.; Duan, X. *Adv. Funct. Mater.* **2015**, *25*, 5006−5015.
(22) Luo, Z.; Yuan, X.; Yu, Y.; Zhang, Q.; Leong, D. T.; Lee, J. Y.; Xie, J. P. *J. Am. Chem. Soc.* **2012**, *134*, 16662−16670.
(23) Goswami, N.; Lin, F.; Liu, Y.; Leong, D. T.; Xie, J. P. *Chem. Mater.* **2016**, *28*, 4009−4016.
(24) Guo, L.; Liang, M. S.; Wang, X. L.; Kong, R. M.; Chen, G.; Xia, L.; Qu, F. L. *Chem. Sci.* **2020**, *11*, 2407−2413.
(25) Rodenas, T.; Luz, I.; Prieto, G.; Seoane, B.; Miro, H.; Corma, A.; Kapteijn, F.; Llabrés I Xamena, F. X.; Gascon, J. *Nat. Mater.* **2015**, *14*, 48−55.
(26) Pan, Y.; Sun, K.; Liu, S.; Cao, X.; Wu, K.; Cheong, W.; Chen, Z.; Wang, Y.; Li, Y.; Liu, Y.; Wang, D.; Peng, Q.; Chen, C.; Li, Y. *J. Am. Chem. Soc.* **2018**, *140*, 2610−2618.
(27) Amiinu, I. S.; Liu, X.; Pu, Z.; Li, W.; Li, Q.; Zhang, J.; Tang, H.; Zhang, H.; Mu, S. *Adv. Funct. Mater.* **2018**, *28*, 1704638.
(28) Zhang, H.; Li, Q.; Liu, R.; Zhang, X.; Li, Z.; Luan, Y. *Adv. Funct. Mater.* **2018**, *28*, 1802830.
(29) Kong, W. S.; Guo, X. X.; Jing, M.; Qu, F. L.; Lu, L. M. *Biosens. Bioelectron.* **2020**, *150*, 111875.
(30) Yang, Q.; Ren, S.; Zhao, Q.; Lu, R.; Hang, C.; Chen, Z.; Zheng, H. *Chem. Eng. J.* **2018**, *333*, 49−57.
(31) Hu, X.; Liu, X.; Zhang, X.; Chai, H.; Huang, Y. *Biosens. Bioelectron.* **2018**, *105*, 65−70.
(32) Fan, C.; Lv, X.; Liu, F.; Feng, L.; Liu, M.; Cai, Y.; Liu, H.; Wang, J.; Yang, Y.; Wang, H. *ACS Sensors* **2018**, *3*, 441−450.
(33) Jia, L.; Chen, X.; Xu, J.; Zhang, L.; Guo, S.; Bi, N.; Zhu, T. *J. Hazard. Mater.* **2021**, *402*, 123776.
(34) Zhao, H.; Liu, F.; Xie, W.; Zhou, T.; OuYang, J.; Jin, L.; Li, H.; Zhao, C.; Zhang, L.; Wei, J.; Zhang, Y.; Li, C. *Sens. Actuators B - Chem* **2021**, *327*, 128899.
(35) Lou, D.; Pang, Q.; Pei, X.; Dong, S.; Li, S.; Tan, W.; Ma, L. *Biosens. Bioelectron.* **2020**, *162*, 112275.
(36) Guan, T.; Huang, W.; Xu, N.; Xu, Z.; Jiang, L.; Li, M.; Wei, X.; Liu, Y.; Shen, X.; Li, X.; Yi, C.; Lei, H. *Sens. Actuators B - Chem* **2019**, *294*, 132−140.
(37) Amirjani, A.; Fatmehsari, D. H. *Talanta* **2018**, *176*, 242−246.
(38) Wang, H.; Da, L.; Yang, L.; Chu, S.; Yang, F.; Yu, S.; Jiang, C. *J. Hazard. Mater.* **2020**, *392*, 122506.
(39) He, L.; Wang, T.; An, J.; Li, X.; Zhang, L.; Li, L.; Li, G.; Wu, X.; Su, Z.; Wang, C. *CrystEngComm* **2014**, *16*, 3259−3263.
(40) Cai, Y.; Qiu, Z. Y.; Lin, X. B.; Zeng, W.; Cao, Y. R.; Liu, W. P.; Liu, Y. J. *Sens. Actuators B - Chem* **2020**, *321*, 128481.
(41) Gao, Q.; Xu, S.; Guo, C.; Chen, Y.; Wang, L. *ACS Appl. Mater. Interfaces* **2018**, *10*, 16059−16065.
(42) Shao, K.; You, J.; Ye, S.; Gu, D.; Wang, T.; Teng, Y.; Shen, Z.; Pan, Z. *Anal. Chim. Acta* **2020**, *1098*, 102−109.
(43) He, L.; Huang, G.; Liu, H.; Sang, C.; Liu, X.; Chen, T. *Sci. Adv.* **2020**, *6*, No. eaay9751.
(44) Zhao, Q.; Chen, S.; Huang, H.; Zhang, L.; Wang, L.; Liu, F.; Chen, J.; Zeng, Y.; Chu, P. K. *Analyst* **2014**, *139*, 1498.
(45) Tao, Y.; Lin, Y.; Huang, Z.; Ren, J.; Qu, X. *Adv. Mater.* **2013**, *25* (18), 2594−2599.

https://doi.org/10.1021/acs.analchem.1c00616
Anal. Chem. 2021, 93, 7275−7282